Supplementary information for "Structural phase purification of bulk HfO_2:Y through pressure cycling"

J. L. Musfeldt [†], [1,2] Sobhit Singh [‡], [3,4] Shiyu Fan,[5] Yanhong Gu,[1] Xianghan Xu,[6,7] S. -W. Cheong,[6,7] Z. Liu,[8] David Vanderbilt,[6] and Karin M. Rabe [*,6]

[1] *Department of Chemistry, University of Tennessee, Knoxville, Tennessee 37996, USA*

[2] *Department of Physics and Astronomy,*
University of Tennessee, Knoxville, Tennessee 37996, USA

[3] *Department of Mechanical Engineering,*
University of Rochester, Rochester, New York 14627, USA

[4] *Materials Science Program, University of Rochester, Rochester, New York 14627, USA*

[5] *National Synchrotron Light Source II,*
Brookhaven National Laboratory, Upton, New York 11973, USA

[6] *Department of Physics and Astronomy,*
Rutgers University, Piscataway, New Jersey 08854, USA

[7] *Rutgers Center for Emergent Materials,*
Rutgers University, Piscataway, New Jersey 08854, USA

[8] *Department of Physics, University of Illinois Chicago, IL 60607-7059, USA*

(Dated: October 2, 2023)

[†] musfeldt@utk.edu

[‡] s.singh@rochester.edu

[*] kmrabe@physics.rutgers.edu

I. Ruby fluorescence reveals pressure + quasi-hydrostatic pressure environment

Figure S1(a) shows a photograph of HfO_2:7%Y inside the gasket of the diamond anvil cell along with an annealed ruby ball and KBr pressure medium. The green 532 nm laser is defocussed to keep the power low and avoid sample damage. Figure S1(b) summarizes the fluorescence of the annealed ruby ball as a function of pressure inside the diamond anvil cell. The $R1$ and $R2$ peaks are well separated and fairly symmetric with increasing pressure, indicating that the sample is in a quasi-hydrostatic environment. Based upon the shape of the fluorescence response as well as the phonon lineshapes, we estimate that the deviation from a perfect hydrostatic pressure environment is on the order of a few percent.

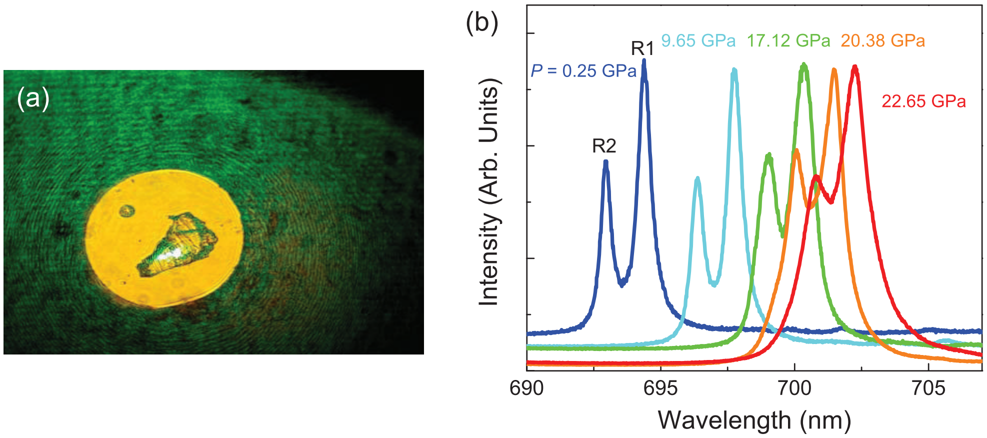

FIG. S1. *(a) Photograph of the sample inside the diamond anvil cell. In addition to* HfO_2*:7%Y, we see the gasket, the ruby ball, the KBr pressure medium, and the defocussed green 532 nm laser. (b) Ruby fluorescence at selected pressures. The lineshapes are reasonable, and the two features are well-separated, consistent with quasi-hydrostatic conditions.*

II. X-ray evidence for the composition of the mixed phase

Figure S2 displays the x-ray diffraction pattern collected on ground powder of as-grown HfO_2:7%Y crystal at 300 K. The calculated diffraction patterns for the monoclinic and orthorhombic phases are shown below for reference in red and green, respectively. A qualitative comparison clearly shows that the as-grown HfO_2:7%Y crystal contains mixed monoclinic and orthorhombic phases. As demonstrated in Ref. [3] of the main text, the orthorhombic phase in the 20 mm/h as-grown crystals with Y concentration ≤11% has an antipolar *Pbca* symmetry. This finding is consistent with TEM results (clear super-lattice peaks due to unit cell doubling) as well. That said, the switching barrier of the antiparallel polarizations is quite high; we see only paraelectric (rather than antiferroelectric) behavior. Therefore, the $x = 11\%$ sample is antipolar but not antiferroelectric.

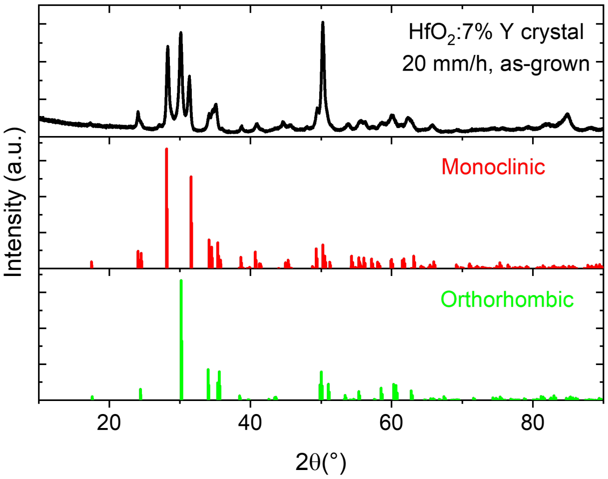

FIG. S2. *Powder x-ray diffraction pattern of as-grown HfO$_2$:7%Y crystal at 300 K and calculated x-ray diffraction patterns of pure monoclinic and orthorhombic phase HfO$_2$. Clearly, the 7% sample is a mixture of the two phases.*

III. Infrared response of HfO$_2$:11%Y under compression

Figure S3 displays the infrared absorption of antipolar orthorhombic HfO$_2$:11%Y as a function of pressure at room temperature. We had hoped that compression might drive this system into the polar orthorhombic phase, but that does not seem to be the case - at least up to 21.5 GPa. Our theoretically-predicted energy diagram [Fig. 5, main text] explains why this is so. A different pressure pathway, perhaps combined with higher temperature or some other tuning parameter, might give a different result.

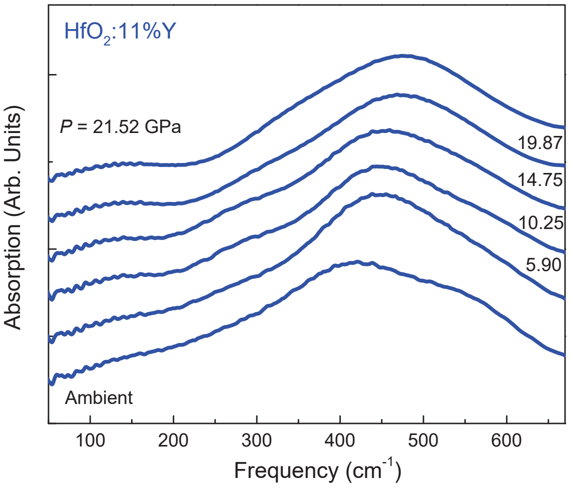

FIG. S3. *Synchrotron infrared absorbance of HfO$_2$:11%Y as a function of pressure at room temperature. The curves are offset for clarity. Pressures to 21.5 GPa do not transform this material to the polar orthorhombic form - consistent with the energy diagram that we discuss in the main text.*

IV. Time and temperature evolution of HfO_2:7%Y after pressure release

Figure S4 summarizes the Raman scattering response of HfO_2:7%Y as a function of time and annealing. The spectrum in Fig. S4(a) was collected more than four months after formation of the antipolar orthorhombic phase. The spectrum is similar to that measured immediately after pressure release [Fig. 1(c), main text], proving that the antipolar orthorhombic phase obtained in this manner is stable over time at room temperature. To investigate whether high temperature impacts the stability of the antipolar orthorhombic phase formed from HfO_2:7%Y, we annealed the sample to 200 ^{o}C in a vacuum oven and then collected the Raman scattering response. The spectrum after annealing is shown in Fig. S4(b) along with the theoretically-predicted result. The features are consistent, demonstrating that the antipolar orthorhombic phase of HfO_2:7%Y is quite stable. This stability extends to both time and temperature.

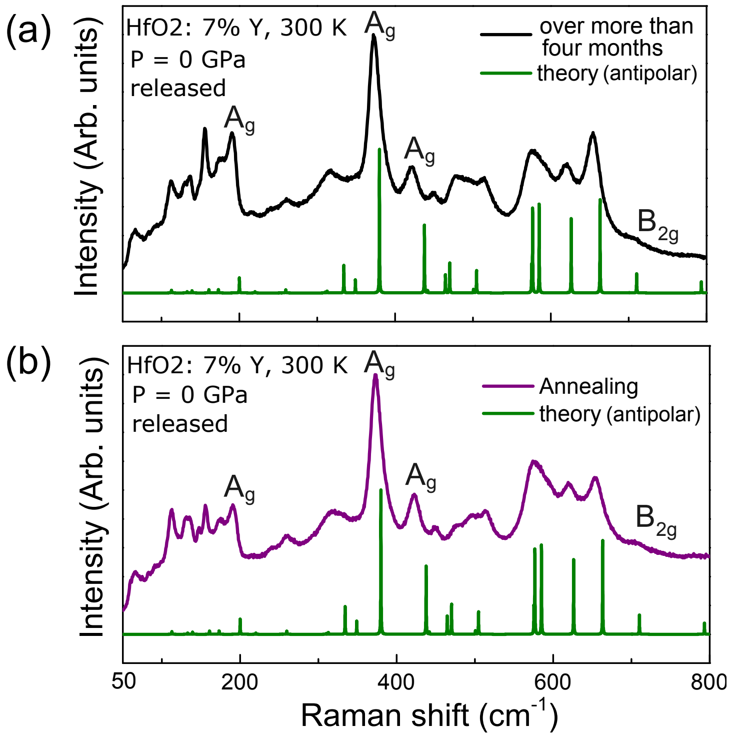

FIG. S4. *(a) Pressure-released Raman spectra of* HfO_2*:7%Y at room temperature more than four months after its original synthesis in the diamond anvil cell. The antipolar orthorhombic phase remains stable. (b) Raman spectrum of* HfO_2*:7%Y after annealing at 200* ^{o}*C in vacuum. The antipolar orthorhombic phase remains stable after annealing. The theoretically-predicted spectrum is shown for comparison in each panel.*

V. Structural parameters of the different phases of hafnia at ambient conditions

TABLE S1. DFT (PBEsol) optimized lattice parameters of different phases of HfO_2 at 0 GPa

Phase	Space group	Cell parameters	Cell angles (Å)
Cubic (c)	$Fm\bar{3}m$ (no. 225)	$a = b = c = 3.547$ Å	$\alpha = \beta = \gamma = 60°$
Tetragonal (t)	$P4_2/nmc$ (no. 137)	$a = b = 3.548$, $c = 5.102$ Å	$\alpha = \beta = \gamma = 90°$
Orthorhombic polar (o-P)	$Pca2_1$ (no. 29)	$a = 5.203$, $b = 5.002$, $c = 5.018$ Å	$\alpha = \beta = \gamma = 90°$
Orthorhombic antipolar (o-AP)	Pbca (no. 61)	$a = 5.022$, $b = 9.944$, $c = 5.197$ Å	$\alpha = \beta = \gamma = 90°$
Monoclinic (m)	$P2_1/c$ (no. 14)	$a = 5.092, b = 5.145, c = 5.261$ Å	$\alpha = \gamma = 90°$, $\beta = 99.83°$

VI. DFT (PBEsol) optimized crystal structures of hafnia at 0 GPa

```
POSCAR: cubic HfO2; spg#225
5.06416000000000
0.0000000000000000 0.4952463073588746 0.4952463073588746
0.4952463073588746 0.0000000000000000 0.4952463073588746
0.4952463073588746 0.4952463073588746 0.0000000000000000
Hf O
1  2
Direct
-0.0000000000000000 -0.0000000000000000 0.0000000000000000
0.2500000000000000 0.2500000000000000 0.2500000000000000
0.7500000000000000 0.7500000000000000 0.7500000000000000
```

```
POSCAR: tetragonal HfO2; spg#137
3.58556000000000
0.9894916179208428 0.0000000000000000 0.0000000000000000
0.0000000000000000 0.9894916179208428 0.0000000000000000
0.0000000000000000 0.0000000000000000 1.4229798649897030
Hf O
2    4
Direct
0.0000000000000000 -0.0000000000000000 0.5000000000000000
0.5000000000000000 0.5000000000000000 0.0000000000000000
0.0000000000000000 0.5000000000000000 0.7914732032298035
0.5000000000000000 0.0000000000000000 0.2085267967701964
0.5000000000000000 0.0000000000000000 0.7085267967701965
0.0000000000000000 0.5000000000000000 0.2914732032298035
```

```
POSCAR: Orthorhombic polar (o-P) HfO2; spg#29
1.00000000000000
5.2034614173910336 0.0000000000000000 0.0000000000000000
0.0000000000000000 5.0017150292844761 0.0000000000000000
0.0000000000000000 0.0000000000000000 5.0184367116197226
Hf O
4 8
Direct
0.5338810611277072 0.2682656345492038 0.2471721366649467
0.4661189388722997 0.7317343654507961 0.7471721366649468
0.0338810611277002 0.7317343654507961 0.2471721366649467
0.9661189388722928 0.2682656345492038 0.7471721366649468
0.8686415587965841 0.0732691926993707 0.1108091866729391
0.1313584412034157 0.9267308073006293 0.6108091866729388
0.3686415587965841 0.9267308073006293 0.1108091866729391
0.6313584412034159 0.0732691926993707 0.6108091866729388
0.2370425263449667 0.4586147668382022 0.9980186766621159
0.7629574736550332 0.5413852331617979 0.4980186766621159
0.7370425263449668 0.5413852331617979 0.9980186766621159
0.2629574736550332 0.4586147668382022 0.4980186766621159
```

```
POSCAR: Orthorhombic antipolar (o-AP) HfO2; spg#61
1.00000000000000
5.0222245873870595 0.0000000000000000 0.0000000000000000
0.0000000000000000 9.9440047872767412 0.0000000000000000
-0.0000000000000000 0.0000000000000000 5.1968880580947001
Hf O
8 16
Direct
0.7449358734204318 0.8849204254227375 0.4638009286482635
0.2550641265795684 0.1150795745772626 0.5361990713517364
0.2449358734204318 0.6150795745772625 0.5361990713517364
0.7550641265795682 0.3849204254227373 0.4638009286482635
0.7550641265795682 0.1150795745772626 0.9638009286482636
0.2449358734204318 0.8849204254227375 0.0361990713517364
0.2550641265795684 0.3849204254227373 0.0361990713517364
0.7449358734204318 0.6150795745772625 0.9638009286482636
0.8718143257415994 0.7906800659868946 0.1246515354238500
0.1281856742584007 0.2093199340131053 0.8753484645761501
0.3718143257415992 0.7093199340131054 0.8753484645761501
0.6281856742584006 0.2906800659868948 0.1246515354238500
0.6281856742584006 0.2093199340131053 0.6246515354238499
0.3718143257415992 0.7906800659868946 0.3753484645761497
0.1281856742584007 0.2906800659868948 0.3753484645761497
0.8718143257415994 0.7093199340131054 0.6246515354238499
0.5023301288055484 0.9766978098509077 0.7614768153239028
0.4976698711944512 0.0233021901490923 0.2385231846760967
0.0023301288055487 0.5233021901490923 0.2385231846760967
0.9976698711944516 0.4766978098509075 0.7614768153239028
0.9976698711944516 0.0233021901490923 0.2614768153239032
0.0023301288055487 0.9766978098509077 0.7385231846760972
0.4976698711944512 0.4766978098509075 0.7385231846760972
```

```
0.5023301288055484 0.5233021901490923 0.2614768153239032
```

```
POSCAR: monoclinic HfO2; spg#14
5.14057000000000
0.9905184186275111 0.0000000000000000 0.0000605440438764
0.0000000000000000 1.0009467791565494 0.0000000000000000
-0.8158286435912250 0.0000000000000000 1.0083163725672586
Hf O
4   8
Direct
0.4294349769234839 0.4571589012168921 0.7069081775355712
0.5705650230765157 0.5428410987831077 0.2930918224644291
0.0705650230765159 0.9571589012168923 0.7930918224644288
0.9294349769234843 0.0428410987831078 0.2069081775355710
0.2709830618181484 0.3362249173108506 0.3416800890201852
0.7290169381818515 0.6637750826891493 0.6583199109798148
0.2290169381818515 0.8362249173108507 0.1583199109798149
0.7709830618181485 0.1637750826891494 0.8416800890201852
0.0343788327232036 0.7579925351179110 0.4816341839411762
0.9656211672767968 0.2420074648820889 0.5183658160588237
0.4656211672767963 0.2579925351179110 0.0183658160588239
0.5343788327232032 0.7420074648820890 0.9816341839411763
```